Impact of Temperature and Optical Error on the Combined Optical and Thermal Efficiency of Solar Tower Systems for Industrial Process Heat

Alexander Zolan[1] [iD], Chad Augustine[2] [iD], Evan Westphal[2] [iD],
Kenneth Armijo[2] [iD], Ye Wang[3] [iD], and John Pye[3] [iD]

[1] National Renewable Energy Laboratory, Golden, CO, United States

[2] Sandia National Laboratories, Albuquerque, NM, United States

[3] Australian National University, Canberra, Australia

Abstract. Concentrating solar thermal (CST) power towers can provide high flux concentrations at commercial scale. As a result, CST towers exhibit potential for high-temperature solar industrial process heat (SIPH) applications. However, at higher operating temperatures, thermal radiation losses can be significant. This study explores the trade-off between thermal and optical losses for SIPH applications using a collection of three case studies at operating temperatures that range from 900-1,550 °C. We assume blackbody radiation to represent the thermal losses at the receiver and we use ray tracing to estimate the optical losses. The results show the impact of process temperature on the maximum attainable system efficiency, as well as the higher flux concentration requirements as the temperature increases.

Keywords: Solar Thermal Tower Systems, Technoeconomic Analysis, Industrial Process Heat

1. Introduction

The Heliostat Consortium (HelioCon) is an ongoing program effort to improve heliostat technology with the objective to drive down costs and increase the performance of solar collection for central receiver, or power tower, concentrated solar thermal (CST) systems [1], [2]. Optical heliostat field enhancements may increase the concentration ratios (CR) achievable at scale for those technologies. Most currently deployed CST systems for industrial process heat (IPH) operate at temperatures lower than 400° C, with applications in textiles, desalination, pharmaceuticals, and food processing [3]. While there is no clear advantage for their use in these lower temperatures, power towers show promise for higher-temperature processes that compose more than 40% of IPH demand as of 2017 [4].

Fernández-González et al. provided a review SIPH research in high-temperature applications, which we define as at least 900 °C in this study, which span metallurgical processes, ceramics production, coatings and surface hardening, and welding and cladding, all of which treat the receiver as a furnace or reaction chamber instead of using thermal energy storage media to transfer heat [5]. Additional work by Lipiński et al. reviews progress in heat transfer to particle storage media for use in future SIPH applications, with a maximum temperature to date of 900 °C [6], illustrating a gap in research of storage and heat transfer for high-temperature SIPH applications.

Our study focuses on the modelling and design of solar tower collection systems for high-temperature SIPH for maximum system efficiency after thermal and optical losses. Compared to the currently deployed electricity-producing tower plants that use molten salt as a heat transfer fluid, thermal losses increase significantly as a function of operating temperature. While this may be mitigated with higher CRs in the system design, the receiver target area is reduced as the CR increases, which leads to increased spillage losses in the solar field. This paper explores the trade-off between these two primary sources of system efficiency loss at a range of temperatures.

Prior work in the HelioCon roadmap report [2] developed three case studies to use as baselines for analysis in HelioCon: (i) a large electric field; (ii) a modular electric field; and, (iii) an SIPH case. In this paper, we more thoroughly investigate SIPH applications by presenting three contrived case studies which are compatible with tower configurations. The case study temperatures of 900, 1200, and 1,550 °C correspond to IPH applications of calcination [7], solar fuels [8], and clinker production [9], respectively. The rest of this paper is organized as follows. Section 2 describes the methodology employed for our study. Section 3 summarizes results and key insights. Section 4 concludes and describes future opportunities for research.

2. Methodology

We model a polar heliostat field aimed at a cavity receiver mounted on a tower. We measure total system efficiency after accounting for black-box radiation losses as a function of the CR. This extends work by Li et al. [10] that determines cost-optimal, temperature-based optical design of solar collection systems with and without a secondary concentrator. In this study, we assume a flat-plate receiver to be the aperture to the cavity receiver. We make as many simplifying assumptions as possible to generalize the results.

This section describes the methodology that we employed to understand the impact of operating temperature and optical error on system efficiency of an SIPH project. Specifically, we describe (i) the modeling framework that we adopted for this analysis, (ii) the blackbody radiation assumption that we adopt as a model for thermal loss at the receiver, (iii) our procedure for determining the maximum-efficiency design, including a justification of removing heliostat size as a design variable.

2.1 SolarPILOT model assumptions

We evaluated the performance of potential plant designs using SolarPILOT [11], a concentrating solar power tower performance characterization tool that includes built-in layout, via the Python API [12]. We use Daggett, California in the United States as the plant location. We assume a radial stagger field layout and a flat-plate receiver target with square, single-facet heliostats that employ center-point aiming; we allow SolarPILOT to select heliostats in the field layout to meet the receiver power design according to annual efficiency estimates using a four-day representative profile. We assume 2 milliradians of slope error on both the horizontal and vertical axes, which is consistent with the baseline study in the HelioCon roadmap and follow-up analysis [13]. To simplify the analysis, we assume no piping losses and only radiation losses at the receiver, the latter of which we describe below in Section 2.2.

2.2 Blackbody radiation assumptions

We use a simplified cavity receiver model that assumes the cavity receiver is an isothermal, perfectly-insulated blackbody, similar to Li et al. [10]. This model assumes that the temperature in the cavity is independent of the heat flux profile incident on the aperture and only depends on the total solar power that enters the cavity receiver through the aperture. Reflective, conductive, and convective losses are assumed to be zero. Steinfeld and Schubnell [14] considered such an ideal windowed cavity. Their work shows that if the absorptance and

emittance for the receiver are assumed to be one, then the receiver acts as a blackbody and radiation losses are a function of the cavity temperature. An idealized receiver with blackbody radiation has long been used as a simplifying assumption for concentrating solar to give an upper or best-case estimate of cavity receiver performance [15], [16]. Blackbody radiation losses are described by the Stefan-Boltzmann equation so that the receiver efficiency is defined in equation (1):

$$\eta_{receiver} = 1 - \sigma T_{receiver}^4 (CR \cdot Flux_{ref})^{-1}, \tag{1}$$

where $\eta_{receiver}$ is the receiver efficiency, or the amount of solar energy collected by the receiver compared to the amount of solar energy entering the receiver aperture, σ is the Stefan-Boltzman constant, $T_{receiver}$ is the isothermal temperature inside the receiver in degrees Kelvin, *CR* is the (unitless) solar concentration ratio, and *Flux*ref is the reference flux, assumed to be 1,000 W/m^2.

The idealized blackbody cavity receiver model was implemented in SolarPILOT by using a square flat plate receiver to represent the cavity receiver aperture. Radiation losses per unit receiver (aperture) area were calculated for the design point CR and calculated at off-design fluxes using the equation (2):

$$Q_{actual} = Q_{design} \left(\frac{CR}{CR_{design}} \right)^{-1} \tag{2}$$

in which Q denotes radiation losses from the receiver. SolarPILOT only allows receiver design losses to be expressed as a 3rd order polynomial, so we approximated *(CR/CR*design)$^{-1}$ using a polynomial expansion.

Figure 1 displays the receiver efficiency as a function of the CR for the three temperatures we use for our case studies, and shows that the flux loss in high-temperature SIPH applications is signficant compared to temperatures currently used for electricity generation; this motivates the study we conduct to obtain the results described in Section 3.
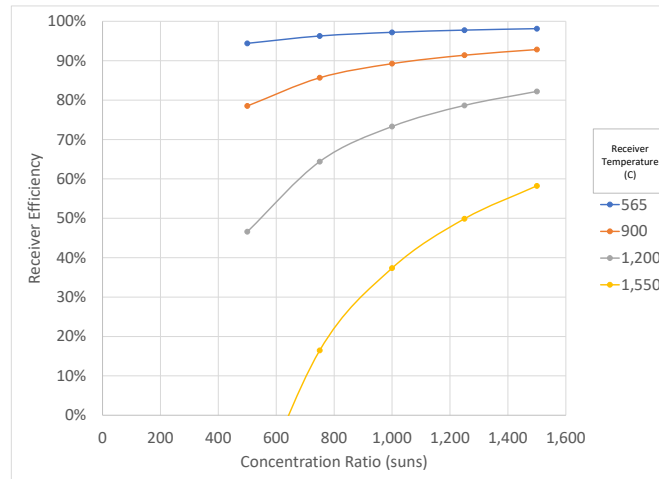

Figure 1. *Summary of a black-body receiver's thermal efficiency as operating temperature and concentration ration vary.*

2.3 Design search parameters

Our study explores the tradeoff between thermal and optical losses at high-temperature SIPH applications by selecting a specific temperature and then varying the design CR of the receiver to target a specific efficiency, $\eta_{receiver}$. Then, for each temperature and design CR pairing, we calculate the (fixed) receiver aperture area, then perform a parameter search to determine a design with near-optimal system efficiency.

We simplify the problem by assuming square receiver apertures and heliostat surfaces and then fixing the ratio of the heliostat height to the receiver height to 0.7 (see Section 2.4). This limits the search space to two dimensions, the tower height and the elevation orientation angle of the receiver aperture, allowing us to search efficiently for a high-quality design. We obtain near-optimal solutions using a grid search that starts with increments of 25 meters in tower height and 10 degrees in elevation angle, then increase resolution and perform a new search around the best-found solution, repeating the procedure until we obtain 1-meter and 1-degree increments for tower heigh and elevation angle, respectively.

2.4 Impact of heliostat size on efficiency

To illustrate the limited impact of heliostat size on the system efficiency and best-found design chosen, we perform a parametric analysis of heliostat size and design CR, the results of which are shown in Figure 2, in which the design CR and best-found system efficiency are shown on the horizontal and vertical axes, respectively. The results show that there is a slight reduction in system efficiency as heliostat size increases, with very limited impact when the heliostat area is smaller than that of the receiver aperture. Moreover, the best-found system's tower height and elevation angle remain consistent as heliostat size changes, indicating that heliostat size has limited impact on both the best design and its system efficiency. To that end, we select a heliostat size with 70 percent of the width and height of the receiver aperture to keep the heliostat size in line with the lower limits of existing designs and increase computational efficiency as compared to smaller sizes. Maintaining this ratio simplifies the analysis as intercept efficiency does not change with solar field size for a given CR.
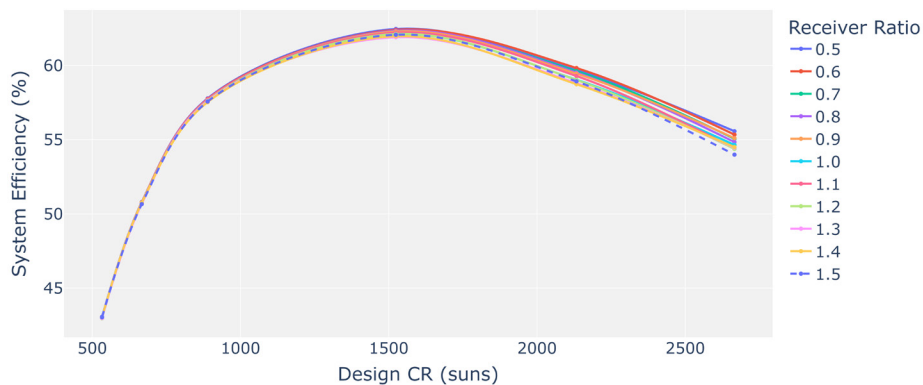

Figure 2. Impact of varying heliostat-to-receiver height ratio for the 20-MW 1,200 °C case.

3. Results

This section summarizes the results of our study. We show design details for all three of our baseline cases, which use 20-MW$_t$ receivers for the three temperatures we selected. We then show the impact of the design CR on efficiency as we vary temperature, power rating, and optical error via parametric analysis.

Table 1 and Figure 3 show key characteristics and solar field layouts for the three baseline case studies that we adopt, respectively. The results show that as the temperature increases, both system efficiency and the receiver aperture decrease, indicating that the CR increases. Additionally, solar field size increases with temperature as more nominal thermal power is delivered to the receiver from the solar field to offset the flux loss at higher temperatures.

Table 1. *Summary of best-found designs for case studies of 20-MW$_t$ SIPH power towers.*

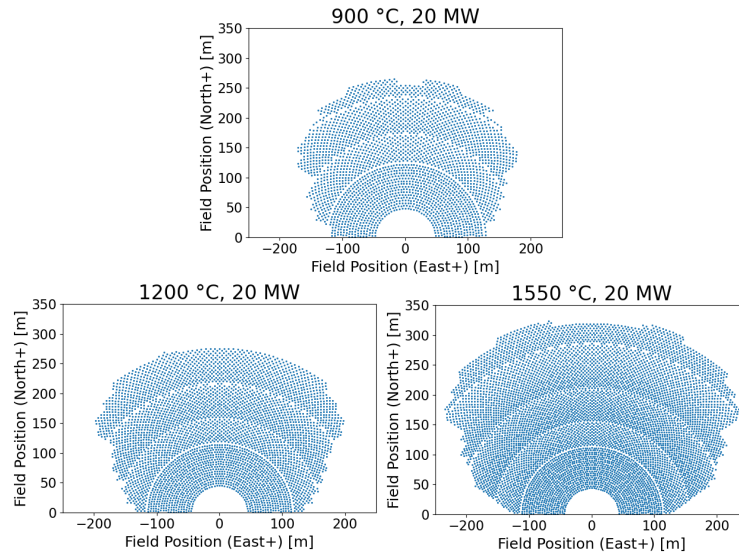|	**900 °C**	**1,200 °C**	**1,550 °C**
Design CR (suns)	1,037	1,471	2,193
Receiver Size (m²)	21.50	16.61	12.76
Heliostat Size (m²)	10.22	7.89	6.07
Total Heliostat Area (m²)	29,794	34,531	44,713
Tower Height (m)	121	113	110
Receiver Elevation Angle	-41	-42	-41
Solar Field Optical Efficiency (%)	81%	76%	67%
Total System Efficiency (including receiver)	73%	63%	48%

Figure 3. *Solar field layouts associated with the maximum-efficiency designs for the three baseline case studies we adopt.*

Figure 4 summarizes the optical and thermal efficiency for each source of loss for the 20-MW$_t$, 1,200 °C case study. This case, as well as the other two which we do not show here, exhibit consistently limited optical losses due to cosine and attenuation, as well as very limited blocking and shading (not shown) due to the radial stagger layout implemented by SolarPILOT. Rather, the two main contributors to efficiency losses are the blackbody radiation and image intercept losses, as higher CRs reduce the latter at the expense of increasing the former.
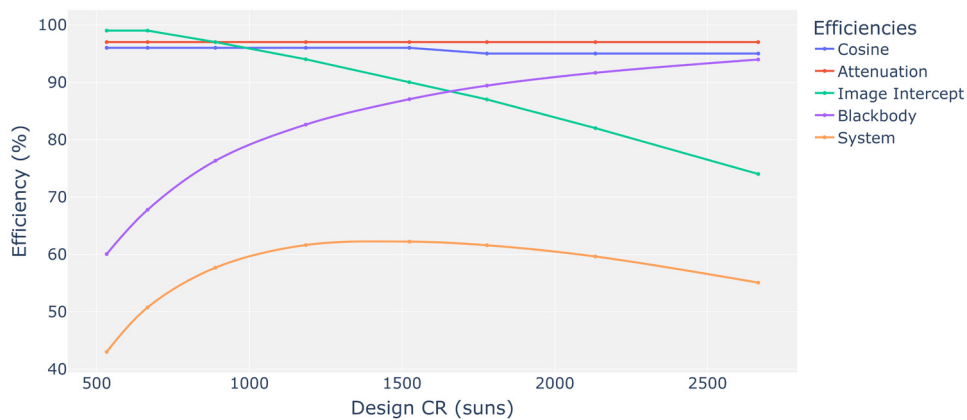

Figure 4. *Summary of optical and thermal efficiencies for the baseline 20-MW 1,200 °C case.*

To understand the impact of the plant size on the best-found efficiency and CR, we conducted a parametric analysis which is summarized in Figure 5; each curve denotes a unique pairing of temperature and receiver thermal power rating. While there is a clear

degradation in system efficiency as the size of the plant increases, the optimal CR remains consistent at each temperature for each receiver power rating. In addition to the results in Figure 5, the receiver elevation angle of the best-found design is consistent, though tower height increases with the power rating. The optimal design CR at the highest temperature is within the range of existing receiver technologies, as sodium receivers have reach flux concentrations of 2.5 MW/m^2 in previous tests [17].
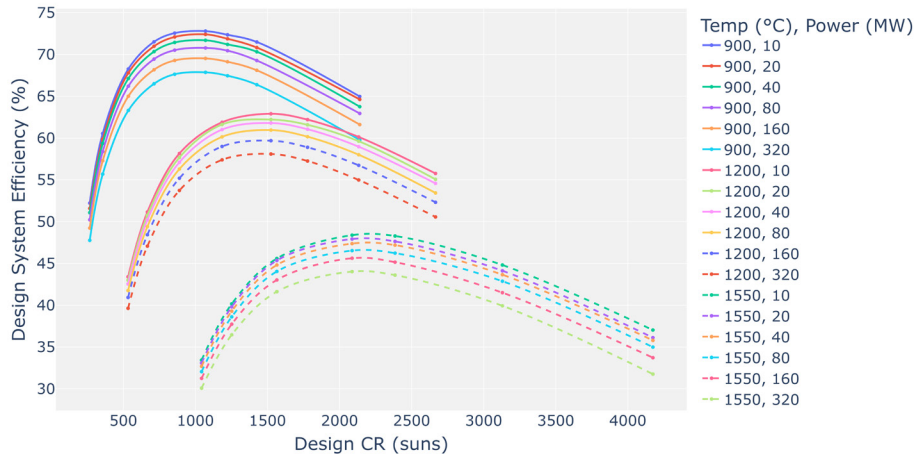

Figure 5. *Summary of best-found system efficiency as temperature, design CR, and plant size vary.*

Figure 6 illustrates the impact of potential optical improvements on the best-found design CR and its related system efficiency for the three case studies. The results show that both the best-found system efficiency and the related optimal CR increase for each temperature as the optical error is improved; this can serve as motivation for ongoing efforts to increase optical precision in heliostat designs.
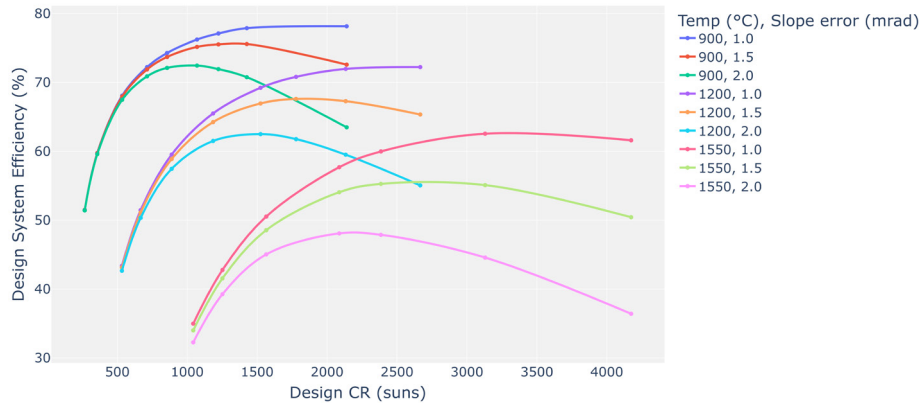

Figure 6. *Comparison of system efficiency as a function of temperature and optical error.*

4. Conclusions

This investigation presents a collection of case studies targeted to SIPH applications that explore the trade-off between image intercept and radiation losses for CST tower designs at temperatures greater than 900 °C. We fixed the heliostat-to-receiver height ratio to 0.7 so that maximum system efficiency could be found by varying only the tower height and receiver elevation angle. Maintaining this ratio simplifies the analysis as intercept efficiency, one of two major sources of efficiency losses in this system, does not change with solar field size for a given CR.

Preliminary results show that increasing CRs to enhance thermal efficiency at the receiver for high-temperature processes come at the cost of optical efficiency losses, even under optimistic assumptions on the minimum allowable receiver target area and heliostat size.

As operating temperature increases, the best obtainable system efficiency decreases, and the required CR to obtain that efficiency level increases. Increasing plant size has limited impact on the best-found design CR. Improvements to optical error increase the optimal CR and the related efficiency, with the upside being strongest at higher temperatures.

Future work will investigate levelized costs using varied cost functions for the tower and receiver, as well as the impact of additional sources of loss at the receiver, such as reflection and advection. The work will explore the optimum size for SIPH heliostat fields as a function of operating temperature.

Data availability statement

The data supporting this analysis can be made available upon request.

Underlying and related material (N/A)

Author contributions

The author contributions are as follows. Alexander Zolan: writing – original draft, investigation, methodology, supervision. Evan Westphal: Investigation, data curation, visualization, software. Chad Augustine: Writing – original draft, investigation, methodology, conceptualization, visualization. Ken Armijo: Writing – review and editing, investigation, methodology. Ye Wang: Writing – review and editing, investigation, validation. Investigation, methodology, validation.

Competing interests

The authors declare that they have no competing interests.

Funding

Acknowledgement

References

1. G. Zhu, "HelioCon: A roadmap for advanced heliostat technologies for concentrating solar power," *Sol. Energy*, vol. 264, p. 111917, Nov. 2023. doi: 10.1016/j.solener.2023.111917.

2. G. Zhu *et al.*, "Roadmap to Advance Heliostat Technologies for Concentrating Solar-Thermal Power," NREL/TP-5700-83041, Sep. 2022. doi: 10.2172/1888029.

3. C. A. Schoeneberger, C. A. McMillan, P. Kurup, S. Akar, R. Margolis, and E. Masanet, "Solar for industrial process heat: A review of technologies, analysis approaches, and

potential applications in the United States," *Energy*, vol. 206, p. 118083, Sep. 2020, doi: 10.1016/j.energy.2020.118083.

4. K. Ravi Kumar, N. V. V. Krishna Chaitanya, and N. Sendhil Kumar, "Solar thermal energy technologies and its applications for process heating and power generation – A review," *J. Clean. Prod.*, vol. 282, p. 125296, Feb. 2021, doi: 10.1016/j.jclepro.2020.125296.

5. D. Fernández-González *et al.*, "Concentrated solar energy applications in materials science and metallurgy," *Sol. Energy*, vol. 170, pp. 520–540, Aug. 2018, doi: 10.1016/j.solener.2018.05.065.

6. W. Lipiński *et al.*, "Progress in heat transfer research for high-temperature solar thermal applications," *Appl. Therm. Eng.*, vol. 184, p. 116137, Feb. 2021, doi: 10.1016/j.applthermaleng.2020.116137.

7. M. Tomatis, H. K. Jeswani, L. Stamford, and A. Azapagic, "Assessing the environmental sustainability of an emerging energy technology: Solar thermal calcination for cement production," *Sci. Total Environ.*, vol. 742, p. 140510, Nov. 2020, doi: 10.1016/j.scitotenv.2020.140510.

8. J.-P. Säck, M. Roeb, C. Sattler, R. Pitz-Paal, and A. Heinzel, "Development of a system model for a hydrogen production process on a solar tower," *Sol. Energy*, vol. 86, no. 1, pp. 99–111, Jan. 2012, doi: 10.1016/j.solener.2011.09.010.

9. F. A. C. Oliveira *et al.*, "Portland cement clinker production using concentrated solar energy – A proof-of-concept approach," *Sol. Energy*, vol. 183, pp. 677–688, May 2019, doi: 10.1016/j.solener.2019.03.064.

10. L. Li, B. Wang, J. Pye, and W. Lipiński, "Temperature-based optical design, optimization and economics of solar polar-field central receiver systems with an optional compound parabolic concentrator," *Sol. Energy*, vol. 206, pp. 1018–1032, Aug. 2020, doi: 10.1016/j.solener.2020.05.088.

11. M. J. Wagner and T. Wendelin, "SolarPILOT: A power tower solar field layout and characterization tool," *Sol. Energy*, vol. 171, pp. 185–196, Sep. 2018, doi: 10.1016/j.solener.2018.06.063.

12. W. T. Hamilton, M. J. Wagner, and A. J. Zolan, "Demonstrating SolarPILOT's Python Application Programmable Interface Through Heliostat Optimal Aimpoint Strategy Use Case," *J. Sol. Energy Eng.*, vol. 144, no. 030906, Mar. 2022, doi: 10.1115/1.4053973.

13. A. Zolan, C. Augustine, and K. Armijo, "Equivalent breakeven installed cost: A tradeoff-informed measure for technoeconomic analysis of candidate heliostat improvements," *Proceedings of 2022 SolarPACES Conference*, 2022, doi: https://doi.org/10.52825/solarpaces.v1i.783.

14. A. Steinfeld and M. Schubnell, "Optimum aperture size and operating temperature of a solar cavity-receiver," *Sol. Energy*, vol. 50, no. 1, pp. 19–25, Jan. 1993, doi: 10.1016/0038-092X(93)90004-8.

15. E. A. Fletcher and R. L. Moen, "Hydrogen- and Oxygen from Water," *Science*, vol. 197, no. 4308, pp. 1050–1056, Sep. 1977, doi: 10.1126/science.197.4308.1050.

16. R. Pitz-Paal, N. B. Botero, and A. Steinfeld, "Heliostat field layout optimization for high-temperature solar thermochemical processing," *Sol. Energy*, vol. 85, no. 2, pp. 334–343, Feb. 2011, doi: 10.1016/j.solener.2010.11.018.

17. W. J. C. Schiel and M. A. Geyer, "Testing an external sodium receiver up to heat fluxes of 2.5 MW/m2: Results and conclusions from the IEA-SSPS high flux experiment conducted at the central receiver system of the Plataforma Solar de Almeria (Spain)," *Sol. Energy*, vol. 41, no. 3, pp. 255–265, Jan. 1988, doi: 10.1016/0038-092X(88)90143-0.